PERGAMON

Quaternary Science Reviews 22 (2003) 1859–1878

QSR

Glacial-interglacial changes in dust deposition on the Chinese Loess Plateau

K.E. Kohfeld*, S.P. Harrison

Max Planck Institute for Biogeochemistry, Postfach 100164, 07701 Jena, Germany

Received 14 July 2001; accepted 31 July 2002

Abstract

The Chinese Loess Plateau (CLP) contains an extensive record of aeolian deposition through multiple glacial–interglacial cycles. Independent chronologies based on pedostratigraphy, magnetic susceptibility, radiocarbon and luminescence dating were developed for 79 sites and used to estimate aeolian mass accumulation rates (MARs) for marine isotope stages 1–5. The regional median value of MAR for Stage 2 is 310 $g/m^2/yr$ compared to an estimate of 65 $g/m^2/yr$ for Stage 5. Estimated MARs from individual sites for Stage 2 are approximately 4.3 times greater than MARs for Stage 5 and 2.1 times greater than for Stage 1. MAR values at individual sites are consistently highest in the northwest and lowest in the southwest of the CLP during all marine isotope stages. MARs estimated on sections through loess terraces are consistently higher than MAR estimates at other sites, indicating that local recycling of loess material from exposed river valley deposits has been significant throughout the last 130 kyr. Although the spatial and temporal patterns in MAR are robust, there are uncertainties about the magnitude of these changes due to (a) lack of bulk density measurements and uncertainties in the chronologies for individual sites, (b) site and chronological biases in the sampling used to derive regional estimates, and (c) the unquantified nature of human impact on accumulation rates during the late Holocene. Nevertheless, the records from the CLP pose a number of challenges which could be addressed by numerical models of the palaeo-dust cycle.

1. Introduction

Loess deposits provide a quasi-continuous record of mineral dust deposition under changing climate regimes. Since loess deposits are generally found in regions close to major dust source areas, they provide a quantitative estimate of changes in the dust cycle that complements ice-core (e.g. Cragin et al., 1977; Hammer, 1977; Fisher, 1979; Petit et al., 1981, 1990, 1999; Hammer et al., 1985; Steffensen, 1997) or marine-core (e.g. Sarnthein and Koopman, 1980; Sarnthein et al., 1981; Clemens and Prell, 1990; Hovan et al., 1991; Sirocko and Lange, 1991; Rea, 1994; Ruddiman, 1997) records of far-travelled dust. This complementarity could be exploited to provide a more rigorous evaluation of model simulations of the palaeo-dust cycle than is currently possible (see e.g. Kohfeld and Harrison, 2001) provided the records can be synthesised at appropriate spatial and temporal scales.

The Chinese Loess Plateau (CLP) is one of the most extensive areas of loess deposition in the world. The CLP spans an area of approximately 440,000 km^2, predominantly in the provinces of Shanxi, Shaanxi and Gansu, between 33–40°N and 98–115°E (Liu, 1985a). The CLP deposits consist of between 100 and 300 m of intercalated loess and palaeosols, formed during alternating cold and warm climate phases (Liu, 1965; Liu et al., 1985; Kukla et al., 1988; Derbyshire et al., 1995). The earliest deposits, the so-called red clay, have been dated to approximately 7 Myr (Sun et al., 1997, 1998a; Ding et al., 1998, 1999; An, 2000) and thus it would appear that the CLP provides a multi-million year record of dust accumulation and climate changes. However, most of the studies carried out on the CLP to date have focussed on records covering recent glacial–interglacial cycles. Although many individual profiles from the CLP have been studied and there is an extensive literature on these records, much of our understanding of changes in dust accumulation during glacial–interglacial cycles is based on a relatively small number of key sites (see e.g. An and Xiao, 1990; An

*Corresponding author. Fax: +49-3641-643-789.
E-mail address: kek@bgc-jena.mpg.de (K.E. Kohfeld).

0277-3791/03/$ - see front matter © 2003 Elsevier Ltd. All rights reserved.
doi:10.1016/S0277-3791(03)00166-5

et al., 1991). This is partly because there has been no comprehensive synthesis of the available records and partly because much of the literature is available only in Chinese.

We have compiled information on 112 sites (5 of which have multiple profiles) on the CLP and from surrounding regions (Sun et al., 2000a). We have used this information to determine aeolian mass accumulation rates over the last five marine isotope stages (i.e. the last 130 kyr). Our goal in this paper is threefold: (a) to document changes in the spatial and temporal patterns of dust deposition on the CLP, (b) to quantify the magnitude of these changes, and (c) to evaluate the potential causes of uncertainties associated with these estimates.

2. Methods

2.1. Site selection

Loess records at individual sites were compiled and documented from the literature (Table 1; Fig. 1a). The sites were classified according to their geomorphological setting, using a standard Chinese classification (Liu, 1964, 1965), because landscape position influences the continuity and thickness of loess deposits. Wide, flat sedimentary basins (yuan sites) represent relatively stable depositional environments and are thus likely to provide the most continuous records and the most reliable estimates of glacial–interglacial changes in dust deposition. We recognised two types of terrace sites; river terrace sites contain loess intercalated with fluvial deposits, while loess terrace sites consist of loess deposited on the top of a river terrace. Both types of terrace site are proximal to local sources that may result in enhanced deposition rates compared to other loess sites. Accumulations of loess on hill slopes are classified as liang- or mao-sites, depending on whether they are elongated or approximately circular. Deposits on hill slopes are likely to be subject to reworking and to contain sedimentary hiatuses. Finally, sections in which loess is intercalated with coarser aeolian deposits were classified as either "desert margin" or "sand dune" sites. Such sites, all of which are located on the northern edge of the CLP, contain multiple hiatuses.

2.2. Calculation of mass accumulation rates

We calculated mass accumulation rates (MARs) for those intervals over which deposition appeared to be continuous at every site (Table 1). MAR material is calculated according to

$$\mathrm{MAR} = \mathrm{AR}^{*}f^{*}\mathrm{BD},$$

where AR is the sediment accumulation rate (m/yr), f is the fraction of sediment that is aeolian, and BD is the sediment bulk density (g/m^3) (Kohfeld and Harrison, 2001). We assume that loess is entirely aeolian and therefore $f=1$.

Published estimates of bulk densities from the CLP range from 1.28 to 1.70 g/cm^3 (Liu, 1966), depending on location and stratigraphic unit (Liu, 1966; Derbyshire et al., 2000). Unfortunately, site-specific bulk density measurements are available for only two sites (Heimugou and Zhangjiayuan). At all other sites across the CLP, we used a bulk density of 1.48 g/cm^2, which is the midpoint of the published values from Liu (1966). Given that the published bulk densities encompass the full range encountered on the CLP, the use of a standard value would impart a maximum error of ca $\pm 15\%$ to our calculations of MAR. Measured bulk densities may be modified by secondary remobilization of carbonate within the loess deposit (An et al., 1991). Unfortunately, without parallel measurements of bulk density and carbonate content, it is not possible to carbonate-normalise bulk density estimates nor is it possible to gauge how large an error carbonate remobilization could impart to our MAR calculations.

The choice of an age model is obviously critical to the estimation of accumulation rates. Several different absolute dating (radiocarbon, luminescence) or stratigraphic correlation (pedostratigraphy, magnetic susceptibility) methods have been used to derive chronologies for loess deposits on the CLP (Fig. 1b). These various methods are often used in combination in order to derive the best-possible chronology at an individual site. As a way of assessing the impact of dating uncertainties on the MAR calculations, we erected independent age models based on each of the different dating techniques available at an individual site. We assumed that the alternation of loess and palaeosols comprising the pedostratigraphic record could be correlated directly to respectively glacial and interglacial stages of the marine isotope stratigraphy of Martinson et al. (1987). Following the geochemical studies of Guo et al. (1993), we assumed that one-third of each palaeosol was formed within the underlying loess and two-thirds was formed by continued deposition of aeolian material during the interglacial intervals. Magnetic susceptibility records have also been used as age models on the CLP (Kukla et al., 1988). We derived an age model by visually aligning the maxima and minima between the bulk magnetic susceptibility records and the Martinson et al. (1987) marine isotope stratigraphy over the last 150 kyr, in order to maximise the R^2 correlation between these records (Paillard et al., 1996). A constant sedimentation rate was then assumed between tie-points. Most of the magnetic susceptibility records are poorly correlated ($R^2 < 0.5$) with the marine isotope stratigraphy, and the highest correlation

Table 1
Site information

Site	Latitude (°)	Longitude (°)	Elevation (m)	Landform	Sources of data	Basis for chronology	References	MAR isotope stages
117 km milestone site	44.28	86.25	1965	Loess terrace	Pedostratigraphy, ^{14}C	None	1	None
Ancun	35.57	106.87	1400	Yuan	Pedostratigraphy, pollen	Pedostratigraphy	1	2, 3, 4, 5
Baicaoyuan	36.27	105.10	2100	Yuan	MS, GS, $CaCO_3$, $\delta^{13}C$, chemical parameters, pedostratigraphy	MS, pedostratigraphy	1	1, 2, 3, 4, 5
Baige	34.80	112.62	90	Loess terrace	Pedostratigraphy, mammal fossil	Pedostratigraphy	1	5
Baimapo	34.17	109.32	650	Yuan	Pedostratigraphy, MS, TL	TL, correlation by MS, pedostratigraphy	1	2, 3, 4, 5
Baishui	35.20	109.59	880	Yuan	MS	MS	1	2, 3, 4, 5
Banshan	34.68	105.70	1400	Yuan	Pedostratigraphy	Pedostratigraphy	1	1, 2, 3, 4, 5
Baoji/Lingyuan	34.33	107.30	970	Yuan	Pedostratigraphy, GS, MS, $\delta^{18}O$, $CaCO_3$, micromorphology	MS, pedostratigraphy	1, 12	1, 2, 3, 4, 5
Baxie/Dongxiang	35.58	103.57	2000	Loess terrace	Pedostratigraphy, MS, GS, $\delta^{13}C$, TOC, ^{14}C, TL	^{14}C TL	1	1, 2
Beiyuan	35.62	103.20	2100	Loess terrace	Pedostratigraphy, MS, GS, ^{14}C, TL, chemical parameters	^{14}C, TL, MS, pedostratigraphy	1, 11	1, 2, 3, 4, 5
Beiyuantou	36.05	107.50	1250	Yuan	MS	MS	1	1, 2, 3, 4, 5
Beizhuangcun/Weinan	34.50	109.50	950	River terrace	Pedostratigraphy, ^{14}C, MS	^{14}C	1	1
Caijiagou/Yulin	38.12	109.83	1250	Loess terrace	Pedostratigraphy, MS, GS, TL, CBD-Fe	TL, pedostratigraphy	1	3, 5
Caocun	34.63	111.15	760	Loess terrace	Pedostratigraphy, MS	Pedostratigraphy	1	1, 5
Caoxian	36.37	104.62	2115	Yuan	Pedostratigraphy, magnetic polarity, MS, GS	Pedostratigraphy	1	5
Chagelebulu_1 (Cagelebulu)	39.88	103.30	1800	Marginal desert site	Pedostratigraphy, pollen, $CaCO_3$, ^{14}C, SiO_2/Al_2O_3	^{14}C	1	1
Chagelebulu_2 (Cagelebulu)	39.88	103.30	1800	Marginal desert site	Pedostratigraphy, ^{14}C	^{14}C	1	1
Changqugou	37.45	108.70	1700	Liang	Pedostratigraphy, MS	Pedostratigraphy	1	5
Changwu	35.20	107.82	1200	Yuan	Pedostratigraphy, MS, chemical parameters	Pedostratigraphy	1	1, 2, 3, 4, 5
Chenjiawo/Lantian_1	34.18	109.48	700	Yuan	Pedostratigraphy, TL, mammal fossil	TL, pedostratigraphy	1	1, 2, 3, 4, 5
Chifeng	42.17	119.02	750	Liang	MS	MS	1	1, 2, 3, 4, 5
Chunhua	34.80	108.55	1100	Yuan	MS	MS	1	1, 2, 3, 4, 5
Dadiwan	35.00	105.92	1400	Loess terrace	Pedostratigraphy, MS, ^{14}C	^{14}C, pedostratigraphy	1	1, 2
Dengkou	40.35	106.95	1100	Marginal desert site	Pedostratigraphy, ^{14}C		1	None
Duanjiapo/Lantian_2	34.20	109.20	700	Yuan	Pedostratigraphy, MS, ^{13}C(organic), ^{13}C(carbonate) ^{18}O(carbonate), magnetic polarity	Pedostratigraphy; MS	1	1, 2, 3, 4, 5

Table 1 *continued*)

Site	Latitude (°)	Longitude (°)	Elevation (m)	Landform	Sources of data	Basis for chronology	References	MAR isotope stages
Dunwashan	35.85	103.25	n/a	Loess terrace	Pedostratigraphy	Pedostratigraphy	1	4, 5
Duobutang	29.36	88.50	3900	Loess terrace	Pedostratigraphy, TL		1	None
Duowa	35.65	102.63	2000	Loess terrace	Pedostratigraphy, OSL, GS, MS	OSL	17	1
Fujiazhuang	36.60	118.50	160	Loess terrace	Pedostratigraphy, TL	Pedostratigraphy	1	5
Ganzi	31.63	99.98	3480	Loess terrace	Pedostratigraphy, magnetic polarity	Pedostratigraphy	1	1, 2, 3, 4, 5
Gaolanshan	36.00	103.83	2135	Loess terrace	Pedostratigraphy, MS, GS, ^{14}C, organic carbon, $CaCO_3$, micromorphology	^{14}C, pedostratigraphy, MS	1	1, 2, 3, 4, 5
Guojialiang	37.50	108.88	1730	Liang	Pedostratigraphy, MS	Pedostratigraphy	1	5
Halali	36.67	99.88	3220	Loess terrace	Pedostratigraphy, ^{14}C, pollen, GS	Pedostratigraphy, ^{14}C	1	1
Heimugou_1 /Luochuan	35.75	109.42	1100	Yuan	Pedostratigraphy, MS, GS, ^{10}Be, phytolith, ^{13}C(organic), ^{13}C(carbonate) ^{18}O(carbonate), magnetic polarity, DBD, $CaCO_3$, chemical parameters, Rb/Sr, sedimentation rate	MS, pedostratigraphy	1, 2, 4, 6	2, 3, 4, 5
Heimugou_2 /Luochuan	35.75	109.42	1100	yuan	Pedostratigraphy, TL	Pedostratigraphy	1	1, 5
Heishan	n/a	n/a	n/a	n/a	^{10}Be, pollen	None	1	None
Heshui	35.82	108.03	1250	Yuan	Pedostratigraphy	Pedostratigraphy	1	5
Huangling	35.60	109.37	1100	Yuan	Pedostratigraphy	Pedostratigraphy	1	5
Huanglong	35.62	109.78	1390	Yuan	MS, GS, CBD-Fe, carbonate content	MS	1, 10	1, 2, 3, 4, 5
Huanxian	36.58	107.35	1270	Yuan	MS, Rb/Sr, pedostratigraphy	MS	1, 2, 6	1, 2, 3, 4, 5
Huining	36.00	105.00	n/a	n/a	Pedostratigraphy	None	7, 20	None
Jiaxian	38.02	110.48	n/a	Marginal desert site	Magnetic polarity; MS; GS; pedostratigraphy; chemical parameters; sedimentation rate	None	8, 9	None
Jiezicun/Jiezhichun	34.33	109.57	650	Yuan	Pedostratigraphy, MS, ^{14}C, TL	^{14}C, TL, MS, pedostratigraphy	1	1, 2, 3, 4, 5
Jingbian	37.59	108.80	n/a	Marginal desert site	GS, stratigraphy, pollen, ^{14}C	None	8, 15	None
Jinjiyuan/Shangzhou	33.90	109.92	950	Loess terrace	Pedostratigraphy, GS, magnetic polarity	Pedostratigraphy	1	5
Jiuzhoutai/Lanzhou	36.07	103.75	2067	Loess terrace	Pedostratigraphy, MS, ^{14}C, TL, magnetic polarity, micromorphology	^{14}C, TL, MS, pedostratigraphy	1	1, 2, 3, 4, 5
Jiyuan	37.15	107.38	1900	Yuan	MS, GS	MS	1	2, 3, 4, 5
Kansu	39.75	75.05	1490	Loess terrace	Pedostratigraphy, TL	Pedostratigraphy	1	5
Landa	36.05	103.84	1510	Loess terrace	Pedostratigraphy, ^{14}C, MS	^{14}C	1	1
Liang Cun/Xi'an	34.47	108.95	950	Loess terrace	Pedostratigraphy, ^{14}C	^{14}C	25	2

Lijiagang	32.17	118.84	70	Loess terrace	MS	None	1	None
Lijiayuan	36.12	104.85	1700	Yuan	MS, GS	MS	1	1, 2, 3, 4, 5
Lingtai/Pingliang	35.07	107.65	1200	Yuan	MS, GS, mammal fossils, magnetic polarity, pedostratigraphy, sedimentation rate	Pedostratigraphy	2, 9, 10, 18, 21	1, 2, 3, 4, 5
Lintaigou	42.03	119.00	1100	Liang	MS	None	1	None
Liping/Dongxiang	35.55	103.58	n/a	River terrace	Pedostratigraphy, ^{14}C	^{14}C	24	1
Liujiapo_1	34.20	109.20	600	Yuan	MS, GS, TL, pedostratigraphy micromorphology	TL, pedostratigraphy	1	2, 3, 4, 5
Liujiapo_2/Xian	34.23	109.12	600	Yuan	Pedostratigraphy	Pedostratigraphy	1	2, 3, 4, 5
Lujiaowan	44.33	85.63	1960	Loess terrace	Pedostratigraphy, ^{14}C, TL	Pedostratigraphy	1	1, 5
Majiayuan	36.27	107.50	1250	Yuan	MS	MS	1	1, 2, 3, 4, 5
Mangshan_1	34.93	113.53	228	Loess terrace	Pedostratigraphy	Pedostratigraphy	1	5
Mangshan_2	34.97	113.37	228	Loess terrace	Pedostratigraphy, OSL, TL, MS, magnetic polarity	OSL, pedostratigraphy	1	1, 2, 3, 4, 5
Mengdashan	35.77	102.00	3200	Loess terrace	Pedostratigraphy	Pedostratigraphy	1	1, 5
Midiwan	37.65	108.62	1400	River terrace	^{14}C, pollen, stratigraphy	None	22	None
Mizhi	37.83	110.08	1100	Mao	Pedostratigraphy, MS	Pedostratigraphy	1	5
Mujiayuan/Wupu	37.57	110.72	1020	Yuan	MS	MS	1	1, 2, 3, 4, 5
Ningxian	35.48	107.97	1200	Yuan	MS	MS	1	1, 2, 3, 4, 5
Niuquanzi	44.18	85.10	1400	Loess terrace	Pedostratigraphy, ^{14}C, TL	Pedostratigraphy	1	3
Potou/Luochuan	35.75	109.42	1090	Yuan	GS, MS, magnetic polarity, pedostratigraphy	Pedostratigraphy	2, 3, 13, 16	1, 2, 3, 4, 5
Pucheng	34.97	109.60	500	Yuan	MS	MS	1	2, 3, 4, 5
Qijidong	29.32	89.20	3900	Loess terrace	Pedostratigraphy, TL	None	1	None
Qinjiazhai	35.74	109.43	1100	Yuan	Pedostratigraphy,^{18}O of quartz, clay minerals	Pedostratigraphy	1	5
Qishan	34.45	107.63	720	Yuan	Pedostratigraphy, MS, $\delta^{13}C$, $\delta^{18}O$, chemical parameters	MS, pedostratigraphy	1	2, 3, 4, 5
Renjiahutong	35.75	109.42	1100	Yuan	Pedostratigraphy, MS, ^{14}C	^{14}C	1	1, 2
Renjiapo	35.02	107.37	1200	Yuan	GS	None	1	None
Salawusu	37.83	108.67	1400	River terrace	Pedostratigraphy, ^{14}C	^{14}C	1	None
Shangjiapo	34.32	108.12	530	Yuan	Pedostratigraphy, micromorphology	Pedostratigraphy	1	2, 3, 4, 5
Shenjiazhuang	36.72	104.13	1900	Loess terrace	Pedostratigraphy, ^{14}C	^{14}C	1	1, 2
Shimao	37.92	110.00	1180	Mao	Pedostratigraphy, TL, MS, GS, CBD-Fe, magnetic polarity	TL, pedostratigraphy	1	5
Shiyaowan	38.80	110.45	1400	Relict sand dune	Pedostratrigraphy, ^{14}C	None	23	None
Taipingchuan_1	44.36	123.24	n/a	Relict sand dune	Pedostratigraphy, IRSL, GLSL	None	14	None
Taipingchuan_2	44.28	123.28	n/a	Relict sand dune	Pedostratigraphy, IRSL, GLSL	None	14	None
Taishanxincun	32.17	118.60	70	Loess terrace	Pedostratigraphy	None	1	None
Tuxiangdao	36.58	101.73	2600	Loess terrace	Pedostratigraphy, MS, GS, $CaCO_3$, TL	TL, pedostratigraphy	1	1, 5
Wangning	37.02	112.95	1100	Loess terrace	Pedostratigraphy, magnetic polarity, MS	None	1	None

Table 1 *continued*)

Site	Latitude (°)	Longitude (°)	Elevation (m)	Landform	Sources of data	Basis for chronology	References	MAR isotope stages
Weinan/Yangguo	34.35	109.52	850	Yuan	Pedostratigraphy, MS, ^{14}C, TL, chemical parameters, micromorphology, ^{10}Be, carbonate, U/Th, CBD-Fe	^{14}C, TL, MS, pedostratigraphy	1	1, 2, 3, 4, 5
Wudangzhao	40.83	110.25	1200	n/a	Pedostratigraphy, ^{14}C	None	1	None
Wuyishan	35.80	103.22	n/a	Loess terrace	Pedostratigraphy	Pedostratigraphy	1	3, 4, 5
Xiadongcun/Jixian	36.10	110.67	1300	Yuan	Pedostratigraphy, MS, GS, magnetic remanence	MS, pedostratigraphy	1	1, 2, 3, 4, 5
Xiaheimu/Luochuan	35.75	109.42	n/a	Yuan	GS, MS	None	2, 3	None
Xi'an_1	34.20	109.20	n/a	n/a	MS, mammal fossils, pedostratigraphy	None	18, 21	None
Xi'an_2/Sanyao	34.28	108.85	n/a	n/a	GS, MS, TL	TL	2, 3	3
Xiangyang/Chenshan	30.87	118.87	150	Loess terrace	Pedostratigraphy, MS, GS	None	1	None
Xiazhupan	37.77	120.66	50	Loess terrace	Pedostratigraphy	None	1	None
Xietongmen	29.43	88.36	3900	Loess terrace	Pedostratigraphy, TL, magnetic polarity	None	1	None
Xifeng_1	35.70	107.70	1330	Yuan	Pedostratigraphy, MS, GS, micromorphology, magnetic polarity, sedimentation rate	MS, pedostratigraphy	1	1, 2, 3, 4, 5
Xifeng_2/Hejiayao/ Hujiayaoxian	35.12	107.00	1350	Yuan	MS, sedimentation rate, magnetic polarity, pedostratigraphy	None	5, 13	None
Xifeng_3/Bajiazui	35.88	107.45	n/a	Yuan	MS, sedimentation rate, pedostratigraphy, magnetic polarity	None	5	None
Xigaze	29.27	88.85	3920	Loess terrace	Pedostratigraphy, TL	None	1	None
Xining/Dadunling	36.63	101.80	2755	Loess terrace	Pedostratigraphy, MS, GS, magnetic polarity	Pedostratigraphy, MS	1	1, 2, 3, 4, 5
Xinzhuangyuan	36.20	104.73	1700	Yuan	MS, GS	MS	1	1, 2, 3, 4, 5
Xuancheng	30.90	118.85	150	Loess terrace	Pedostratigraphy, MS, ^{13}C, chemical parameters	None	1	None
Xuanheze	37.65	108.62	1400	River terrace	Pedostratigraphy, ^{14}C	None	23	None
Xueyuan	36.92	106.97	1650	Yuan	MS	MS	1	1, 2, 3, 4, 5
Xunyi	35.13	108.33	1200	Yuan	MS, sedimentation rate	MS	1, 2	1, 2, 3, 4, 5
Yanchang	36.60	110.02	1040	Yuan	MS, GS, CBD-Fe, carbonate content	MS	1, 10	1, 2, 3, 4, 5
Yangjiashan/Fenzhou	34.00	106.65	1600	Loess terrace	Pedostratigraphy, GS, magnetic polarity	Pedostratigraphy	1	2, 3, 4, 5
Yangmeitang	32.17	118.84	n/a	n/a	MS	None	1	None
Yangtaomao	38.80	110.45	1400	Relict sand dune	Pedostratigraphy, MS, GS, ^{14}C, organic matter	None	1, 26	None
Yanziji	32.15	118.82	70	Loess terrace	Pedostratigraphy, TL	None	1	None
Yichuan	36.13	110.15	1017	Yuan	MS, pedostratigraphy, chemical parameters, GS, CBD-Fe, carbonate content	MS	1, 10	1, 2, 3, 4, 5

Yinwan	34.93	104.17	2100	Loess terrace	Pedostratigraphy, MS, GS, organic matter, $CaCO_3$, ^{14}C, TL	^{14}C	1	1
Yuanpu (Yuanbo)	35.63	103.17	2100	Yuan	Pedostratigraphy, pollen, MS, ^{14}C, GS, $CaCO_3$	^{14}C, MS, pedostratigraphy	1	1, 2, 3, 4, 5
Yulin (Yuling)	38.35	109.70	1200	Marginal desert site	Pedostratigraphy, ^{14}C	^{14}C	1	1
Zhaitang	39.98	115.68	150	Loess terrace	Pedostratigraphy, ^{14}C , TL, GS	Pedostratigraphy	1	1, 2, 3, 4, 5
Zhangjiayuan	34.27	107.83	550	Yuan	Pedostratigraphy, GS, DBD and other mechanic parameters	Pedostratigraphy	1	1, 2, 3, 4, 5
Zhengbeidai (Zhengbeitai)	38.35	109.70	n/a	Marginal desert site	Pedostratigraphy, ^{14}C	^{14}C	24	1
Zihedian	36.78	118.37	120	Loess terrace	Pedostratigraphy, TL	None	1	None

A version of this table in which site names are also listed in Chinese characters can be obtained from the first author.
MS, magnetic susceptibility; GS, grain size; TL, thermoluminescence; OSL, optically stimulated luminescence; IRSL, infrared optically stimulated luminescence; GLSL, green light stimulated luminescence; ^{14}C, radiocarbon dating, ^{10}Be, Beryllium-10 dating; TOC, total organic carbon; DBD, dry bulk density; CBD-Fe, "citrate-bicarbonate-dithionite" extracted Fe; mechanical parameters, void ratio, porosity, liquid limit, plastic limit, plastic index.
References: 1 = Sun et al. (2000a) and references therein; 2 = An (2000); 3 = An and Porter (1997); 4 = An and Sun (1995); 5 = An et al. (1999); 6 = Chen et al. (1999); 7 = Ding et al. (1991); 8 = Ding et al. (1998); 9 = Ding et al. (1999); 10 = Ding et al. (2001); 11 = Fang et al. (1996); 12 = Gu et al. (1997); 13 = Kukla and An (1989); 14 = Lai et al. (1999); 15 = Liu et al. (1996); 16 = Lu et al. (1999); 17 = Roberts et al. (2001); 18 = Sun et al. (1997); 19 = Sun et al. (1998b); 20 = Sun et al. (1999); 21 = Zheng et al. (1992); 22 = Zhou et al. (1996); 23 = Zhou et al. (1997); 24 = Zhou et al. (1998); 25 = Zhou et al. (1999b); 26 = Zhou et al. (1999a).

obtained was only 0.77 (Sun et al., 2000a). Improved correlations might be obtained by extending the comparison over several glacial–interglacial cycles. Nevertheless, the relatively weak correlations obtained between individual magnetic susceptibility records and the marine isotope stratigraphy suggests a need for caution when using magnetic susceptibility as a dating tool on the CLP, a finding supported by recent attempts to refine the astronomic timescale for Chinese loess deposits (Heslop et al., 2000).

We used linear interpolation between adjacent dates on continuous sediments to erect age models for both radiocarbon and luminescence dates. However, we used only those radiocarbon dates or luminescence dates, which passed a rigorous quality control test. Specifically:

(1) when adjacent dates overlapped (within the standard deviation), the date with the largest standard deviation was rejected and not used in the age model;
(2) dates associated with an age reversal were rejected and not used in the age model. In situations where it was unclear which of the dates was reversed, the date with the largest standard deviation was rejected;
(3) dates which were suspected of contamination by the original authors were not used to erect the age model; and
(4) dates with a standard deviation of >2000 years (in the case of radiocarbon) and $>10\%$ (in the case of luminescence) were rejected and not used in the age model.

Radiocarbon dates were converted to calendar years, using the CALIB 4.1 software (Stuiver and Reimer, 1993; Stuiver et al., 1998a, b), prior to the creation of the age model. As a result, dates older than 20,265 radiocarbon yr B.P. are not taken into consideration in the age models. Although there is still some debate about the maximum age limit for luminescence dating (see e.g. Berger, 1988; Berger et al., 1992; Wintle, 1993a, b, 1997; Wintle et al., 1993; Aitken, 1998), the consensus appears to be that ages of $>130{,}000$ yr on bulk samples of heterogeneous material are unreliable. We therefore excluded all luminescence dates $>130{,}000$ yr prior to erecting the age models at individual sites.

At every site, we made estimates of MAR for any dated interval for which there was continuous sedimentation. In the case of the age models based on pedostratigraphy or magnetic susceptibility, we were necessarily confined to estimating the average accumulation rate over each of the marine isotope stages (i.e. Stage 1: 1–12 kyr BP; Stage 2: 12–24 kyr BP; Stage 3: 24–59 kyr BP; Stage 4: 59–74 kyr BP; Stage 5: 74–130 kyr BP). MAR estimates covering more limited time periods were possible using the age models based on absolute dating methods. However, to facilitate

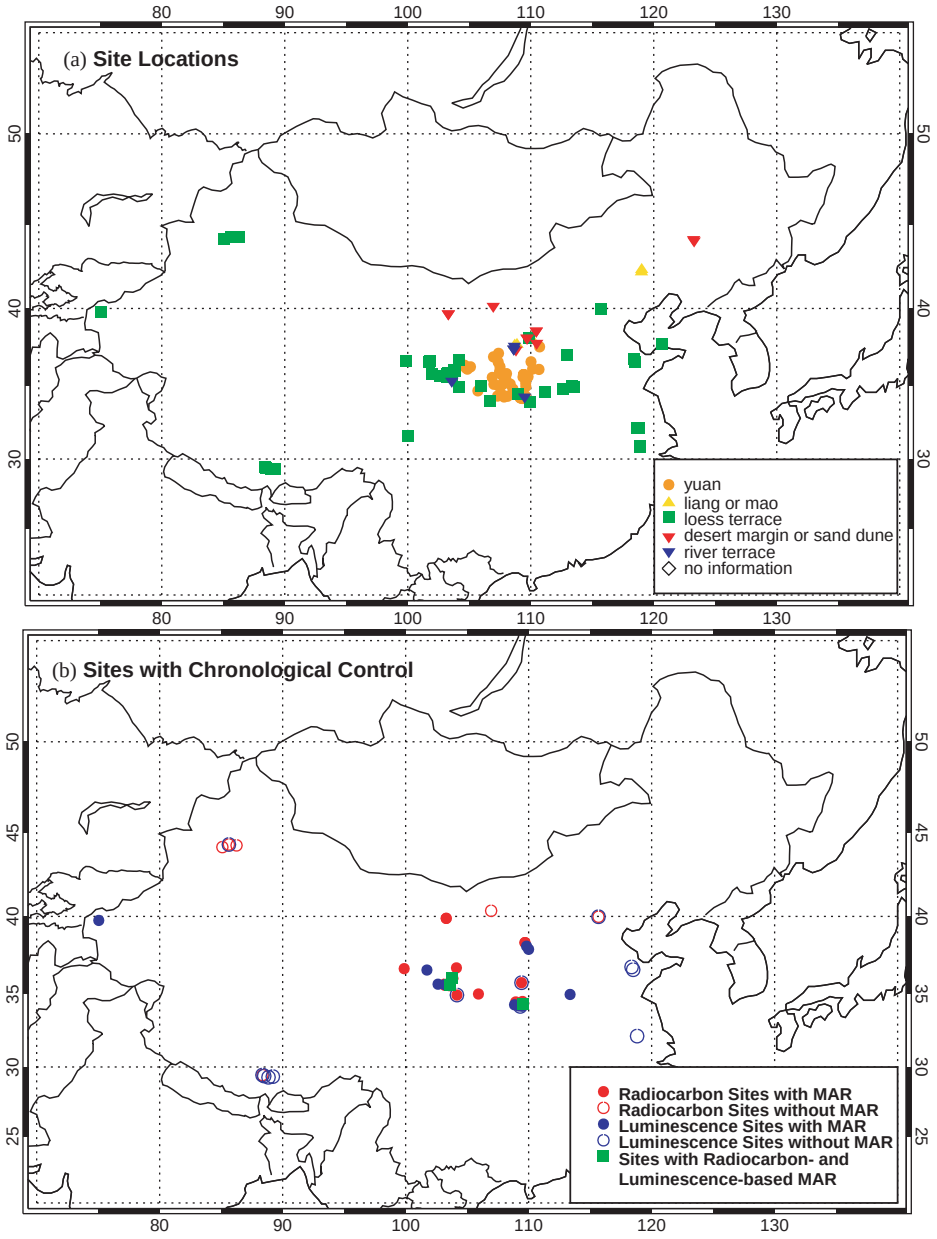

Fig. 1. Sites from the CLP (a) classified by geomorphic setting, and (b) at which MARs have been estimated for at least one stage based on absolute dating techniques. Solid red and blue symbols indicate sites where MAR has been estimated for at least one stage using respectively radiocarbon and luminescence dating techniques. Solid green squares represent sites where MAR was calculated for at least one stage using both radiocarbon and luminescence dating independently. Open red and blue symbols show sites where the available radiocarbon and luminescence dates (respectively) are insufficient to estimate a MAR for any stage.

comparisons between the various types of age model, we also made estimates of the average accumulation rate during each of the marine isotope stages based on radiocarbon and luminescence dating.

3. Results

Only 79 of the 112 sites originally investigated proved suitable for generating records of MAR. Many of the other sites were in unsuitable geomorphic locations and therefore had discontinuous records or had undergone extensive reworking. Other records were excluded from our analyses because they were inadequately dated or inadequately documented in the original publication. Although the CLP is a relatively well-studied region, there are relatively few sites for which it is possible to derive comprehensive and independent chronologies based on absolute dating methods (Fig. 1b). Only 14 of the subset of 79 sites in our data set for which it was possible to calculate MARs had sufficient reliable luminescence dates to generate a MAR for any time

period. Only 18 of the 79 sites had sufficient reliable radiocarbon dates to generate a MAR for any time period. Thus, most of the records from the CLP are dated using age models that assume direct synchroneity between soil formation, magnetic susceptibility and changes in global ice volume. Given the generally poor correlations between the magnetic susceptibility records from the CLP and the marine isotope stratigraphy, and the fact that our assumption about the importance of continued loess deposition during soil-forming intervals is based on a single geochemical study, the reliance on correlation-dating techniques could be problematic.

Aeolian MARs for each isotope stage are non-normally distributed. For Stage 2, for example, the mean is $479 \pm 726\,g/m^2/yr$. The large standard deviation suggests that the mean value is largely influenced by a small number of outliers, resulting in an average that is greater than 75% of the samples for Stage 2. Because of this asymmetrical distribution we use the median value as a more robust representation of the regional MAR for each stage.

Interglacial and interstadial periods (Stages 1, 3 and 5) have lower MARs than glacial periods (Stages 2 and 4) (Fig. 2). The highest MARs at individual sites are recorded for Stage 2 (Table 2). The median MAR during Stage 2 is $310\,g/m^2/yr$. This is virtually identical to the value obtained for Stage 4 ($309\,g/m^2/yr$) but 4.8 times greater than the value for Stage 5 ($65\,g/m^2/yr$) and 1.8 times greater than that for Stage 1 ($171\,g/m^2/yr$). The median MAR for Stage 1 is, in fact, higher than that obtained for interstadial Stage 3 ($154\,g/m^2/yr$). Although the range of values for each stage is large, the patterns of change between stages appear rather robust. Thus, comparison of the maximum or minimum MAR registered during specific stages (Table 2) also shows glacial stages as intervals of enhanced dust accumulation, and Stage 5 as the time of lowest dust accumulation on the CLP.

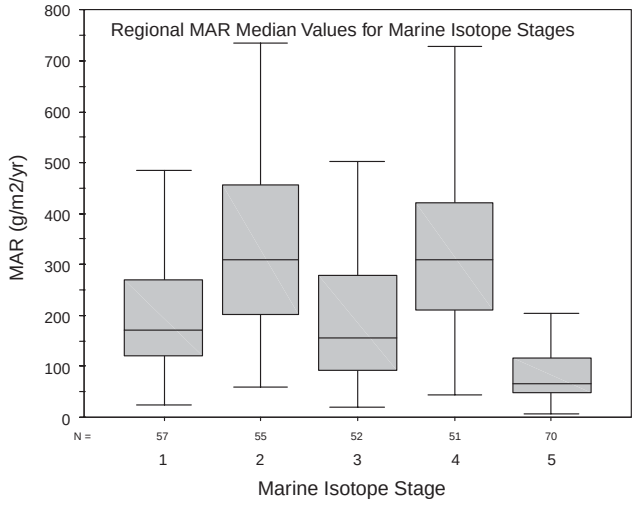

Fig. 2. MAR ($g/m^2/yr$) estimates for marine isotope stages 1–5, estimated using box-and-whisker plots, where the upper and lower lines of the box represent the 75th and 25th percentiles, respectively. Thus the box represents the middle 50%, or interquartile range, of the data. The line in the middle of the box is the sample median, and the lines above and below the box show the maximum and minimum values for each stage. Outliers, which are greater than 1.5 times the interquartile range, are not shown. MARs for each sample site are averaged based on all age models available at that site. Numbers at the bottom of each column indicate the number of samples for each stage.

Notwithstanding the apparent robustness of changes in MAR in qualitative terms, there are substantial differences in the estimated MAR depending on the dating method used to erect age models at individual sites (Fig. 3; Table 3). The median MAR for Stage 1 ranges from $128\,g/m^2/yr$ (pedostratigraphy, $N=26$) to $144\,g/m^2/yr$ (magnetic susceptibility, $N=26$) to $463\,g/m^2/yr$ (radiocarbon, $N=18$), to $846\,g/m^2/yr$ (luminescence, $N=2$). Similarly, the median MAR for Stage 2 ranges from $257\,g/m^2/yr$ (magnetic susceptibility, $N=34$) to $345\,g/m^2/yr$ (pedostratigraphy, $N=25$) to $361\,g/m^2/yr$ (absolute dating methods, $N=12$). Pedostratigraphic and magnetic susceptibility dating techniques, based on correlation with the marine isotope record, tend to emphasise glacial–interglacial differences in MAR; absolute dating techniques (radiocarbon, luminescence dating) suggest glacial–interglacial changes were smaller.

Estimated MARs are highest at sites in the northwest of the CLP and lowest in sites in the southeast (Fig. 4) during all five marine isotope stages. Such a pattern is consistent with a dust source to the northwest of the CLP and the persistence of a broadly similar trajectory for dust transport over the last interglacial–glacial–interglacial cycle (Derbyshire et al., 1998). Again, the existence of a spatial gradient in MAR is a robust feature of the data although the absolute magnitude of the changes is critically dependent on the dating technique used to erect age models at individual sites.

The geomorphological setting also has a significant impact on the MAR estimate at individual sites (Fig. 5; Table 4). Loess terrace sites have higher MARs than non-terrace sites. The median Stage 2 MAR from terrace sites is $637\,g/m^2/yr$, compared with an estimate of $262\,g/m^2/yr$ from non-terrace sites. The median Stage 4 MAR from terrace sites is $648\,g/m^2/yr$, compared to $281\,g/m^2/yr$ from non-terrace sites. Thus, during glacial periods the MAR estimated from terrace sites is more than twice that from non-terrace sites. During interglacial/interstadial periods, the difference between terrace and non-terrace sites is smaller. The estimated Stage 1 and Stage 3 MARs from terrace sites are less than that for non-terrace sites, and median Stage 5 MARs for terrace and non-terrace sites are approximately the same. Thus, glacial–interglacial differences in

Table 2
Average aeolian mass accumulation rates ($g/m^2/yr$) estimated for all data

Site	Longitude	Latitude	Stage 1	Stage 2	Stage 3	Stage 4	Stage 5	Ratio 2/1	Ratio 2/5
Ancun	106.87	35.57			180	309	41		
Baicaoyuan	105.10	36.27	144	335	470	253	154	2.1	2.2
Baige	112.62	34.80					18		
Baimapo	109.32	34.17		153	89	131	28		4.1
Baishui	109.59	35.20		69	62	44	83		0.8
Banshan	105.70	34.68	164	366	54	289	76	2.2	4.8
Baoji/Lingyuan	107.30	34.33	111	179	128	206	50	1.7	4.5
Baxie/Dongxiang	103.57	35.58	1298	944				0.4	
Beiyuan	103.20	35.62	159	863	491	726	261	6.0	6.3
Beiyuantou	107.50	36.05	81	468	185	331	75	5.8	6.2
Beizhuangcun/Weinan	109.50	34.50	574						
Caijiagou/Yulin	109.83	38.12			345		134		
Caocun	111.15	34.63	262				70		
Caoxian	104.62	36.37					153		
Chagelebulu_1 (Cagelebulu)	103.30	39.88	506						
Chagelebulu_2 (Cagelebulu)	103.30	39.88	387						
Changqugou	108.70	37.45					72		
Changwu	107.82	35.20	251	304	39	332	42	1.2	7.2
Chenjiawo/Lantian_1	109.48	34.18	25	345	100	194	21	13.8	16.4
Chifeng	119.02	42.17	136	237	154	346	139	1.7	1.7
Chunhua	108.55	34.80	147	168	215	198	67	1.1	2.5
Dadiwan	105.92	35.00	1048	348					
Duanjiapo/Lantian_2	109.20	34.20	142	159	71	128	28	1.1	5.8
Dunwashan	103.25	35.85				2113	223		
Duowu	102.63	35.65	244						
Fujiazhuang	118.50	36.60					18		
Ganzi	99.98	31.63	164	514	56	312	53	3.1	9.7
Gaolanshan	103.83	36.00	294	1277	347	1027	116	4.4	12.7
Guojialiang	108.88	37.50					140		
Halali	99.88	36.67	268						
Heimugou_1/Luochuan	109.42	35.75		274	124	281	59		3.8
Heimugou_1/Luochuan	109.42	35.75	116	250	98	214	57	2.2	4.4
Heimugou_2	109.42	35.75	131				46		
Heshui	108.03	35.82					49		
Huangling	109.37	35.60					35		
Huanglong	109.78	35.62	67	97	130	187	75	1.4	1.3
Huanxian	107.35	36.58	169	339	501	565	109	2.0	3.1
Jiezicun/Jiezhichun	109.57	34.33	203	187	155	86	94	1.0	2.9
Jinjiyuan/Shangzhou	109.92	33.90					11		
Jiuzhoutai/Lanzhou	103.75	36.07	664	637	472	570	563		3.2
Jiyuan	107.38	37.15		532	809	692	171		3.1
Kansu	75.05	39.75					18		
Landa	103.84	36.05	296						
Liang Cun/Xi'an	108.95	34.47		205					
Lijiayuan	104.85	36.12	180	340	455	385	146	1.9	2.3
Lingtai/Pingliang	107.65	35.07	95	294	42	281	63	3.1	4.7
Lintaigou	119.00	42.03							
Liping/Dongxiang	103.58	35.55	1016	1064				1.0	
Liujiapo_1	109.20	34.20		105	127	226	48		
Liujiapo_2/Xian	109.12	34.23		107	55	89	51		2.1
Lujiaowan	85.63	44.33	125				6		
Majiayuan	107.50	36.27	138	420	340	296	90	3.0	4.7
Mangshan_1	113.53	34.93					30		
Mangshan_2	113.37	34.97	214	5238	473	2279	1330	24.5	13.3
Mengdashan	102.00	35.77	512				50		
Mizhi	110.08	37.83					95		
Mujiayuan/Wupu	110.72	37.57	166	205	252	380	69	1.2	3.0
Ningxian	107.97	35.48	187	200	211	252	68	1.1	2.9
Niuquanzi	85.10	44.18			21				
Potou/Luochuan	109.42	35.75	84	310	100	344	52	3.7	6.0
Pucheng	109.60	34.97		60	83	95	16		3.8
Qishan	107.63	34.45		208	91	113	34		6.8

Table 2 (*continued*)

Site	Longitude	Latitude	Stage 1	Stage 2	Stage 3	Stage 4	Stage 5	Ratio 2/1	Ratio 2/5
Renjiahutong	109.42	35.75	219	241				1.1	
Shangjiapo	108.12	34.32		341	177	312	29		11.8
Shenjiazhuang	104.13	36.72	442	442				1.0	
Shimao	110.00	37.92					193		
Tuxiangdao	101.73	36.58	90				170		
Weinan/Yangguo	109.52	34.35	207	289	123	184	63	1.8	4.9
Wuyishan	103.22	35.80			140	1022	62		
Xiadongcun/Jixian	110.67	36.10	71	229	136	319	47	3.2	4.8
Xiadongcun/Jixian	110.67	36.10	239	151	168	226	47	0.6	3.2
Xi'an_2/Sanyao	108.85	34.28	58	343	146	395	73	5.9	4.7
Xifeng_1	107.70	35.70	122	372	168	302	85	3.2	4.3
Xining/Dadunling	101.80	36.63	171	733	269	435	175	5.4	4.4
Xinzhuangyuan	104.73	36.20	171	486	609	611	204	2.8	2.4
Xueyuan	106.97	36.92	121	514	258	540	144	4.2	3.6
Xunyi	108.33	35.13	113	130	171	197	83	1.2	1.6
Yanchang	110.02	36.60	95	212	285	410	56	2.2	3.8
Yangjiashan/Fenzhou	106.65	34.00			113	358	63		
Yichuan	110.15	36.13	172	200	210	216	76	1.2	2.6
Yinwan	104.17	34.93	619	285				0.5	
Yuanpu (Yuanbo)	103.17	35.63	208	1055	429	954	202	6.8	6.7
Yulin (Yuling)	109.70	38.35	485						
Zhaitang	115.68	39.98	25	407	31	510	18	16.3	22.6
Zhangjiayuan	107.83	34.27	74	370	70	299	55	5.0	6.7
Zhengbeidai (Zhengbeitai)	109.70	38.35	1426	1719				1.2	
Statistics									
Median			171	310	154	309	65	2.1	4.25
Average			279	479	212	423	106	4	5
SD			297	726	170	425	170	5	4
max			1426	5238	809	2279	1330	24	23
min			25	60	21	44	6	0	1
N			57	55	52	51	69	43	46

MARs are greatly amplified at loess terrace sites compared with non-terrace sites (Fig. 6).

Our analyses demonstrate the existence of broad-scale temporal and spatial patterns in MAR. However, analyses of records from Stage 1 with multiple absolute dates ($N = 12$) show that there is considerable millennial-scale variability in dust accumulation (Fig. 7). Dust accumulation appears to have been high during the late glacial and early Holocene. Minimum dust accumulation at all sites occurred between 6000 and 3000 yr B.P. The changes in MAR are substantial: the average MAR at 9 kyr is 764 g/m^2/yr compared to 478 g/m^2/yr at 4 kyr.

4. Discussion

4.1. Glacial/interglacial changes in MARs

Ice core and marine core records document a significant increase in the vigour of the atmospheric dust cycle during glacial climates compared to interglacial climates (Thompson, 1977; Thiede, 1979; Petit et al., 1981; Sarnthein et al., 1981; De Angelis et al., 1984; Rea, 1990, 1994; Ruddiman, 1997; Steffensen, 1997). Glacial periods are also coincident with the emplacement of most of the northern-hemisphere loess deposits (e.g. Pye, 1987; Frechen and Dodonov, 1998; Muhs et al., 1999). The increased vigour of the dust cycle is a result of the colder, drier and windier glacial climate and the consequent reduction in vegetation cover and expansion of dust source areas (Mahowald et al., 1999; Reader et al., 1999, 2000). Several lines of evidence suggest that conditions were more arid over much of central Asia during the last glacial period, leading to expansion of potential dust source areas. Pollen records from central Europe (Elenga et al., 2000), central Asia (Tarasov et al., 2000) and from China (Yu et al., 2000; Harrison et al., 2001b) indicate that the area of desert and relatively sparse steppe or steppe–tundra vegetation was greater compared to today. Stratigraphic studies from the Mu Us desert indicate episodic expansions of the desert during Stage 4 to 2, with the last such expansion occurring between 27 and 10 kyr B.P. (Sun et al., 1998c). The lake-level record from central Asia is more equivocal, but at least some sites in

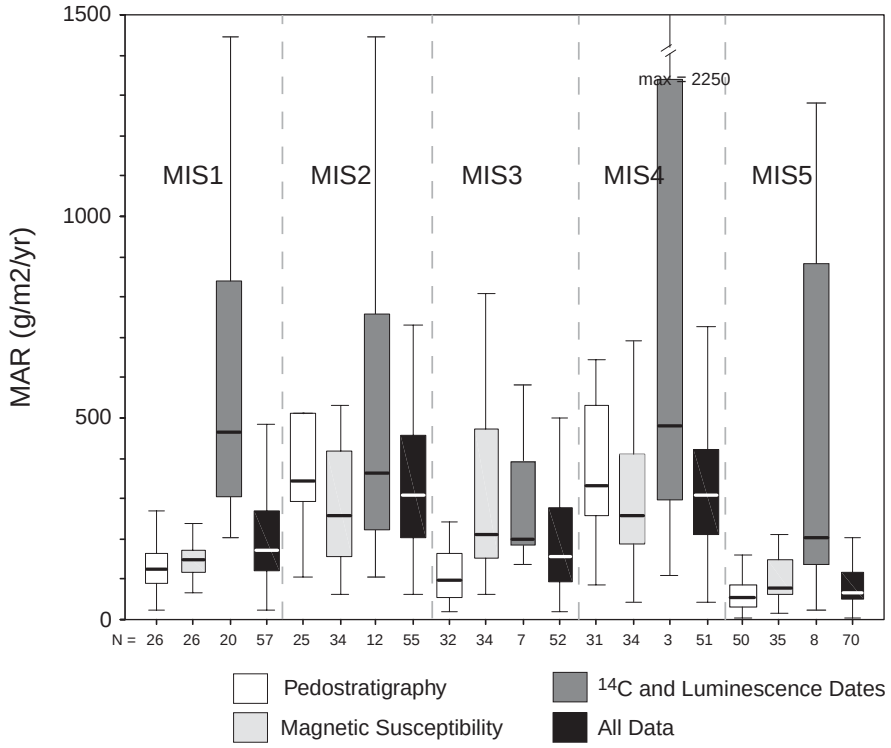

Fig. 3. Regional estimates of MAR for marine isotope stages 1–5 based on all sites compared with sites in which the chronologies were based on pedostratigraphy, magnetic susceptibility or absolute-dating techniques respectively. Box-and-whisker presentation as in Fig. 2. Numbers at the bottom of each column indicate the number of samples.

Table 3
Regional mass accumulation rates ($g/m^2/yr$) for different age model types

	Stage	Median	Mean	min	max	*N*
Pedostratigraphy	1	128	150	25	512	26
	2	345	693	107	5238	25
	3	98	129	21	500	32
	4	332	535	86	2355	31
	5	52.5	78	6	395	50
Magnetic susceptibility	1	144	149	67	270	26
	2	257	318	60	1369	34
	3	210	286	62	809	34
	4	332	535	86	2355	31
	5	52.5	78	6	395	50
Dates	1	463	600	203	1449	20
	2	361	571	105	1719	12
	3	201	296	137	582	7
	4	481	981	110	2202	3
	5	202	591	24	2265	8
Average (all data)	1	171	279	25	1426	57
	2	310	478	60	5238	55
	3	154	212	21	809	52
	4	309	422	44	2279	51
	5	65	106	6	1330	70

northwestern China indicate increased regional aridity during the last glacial maximum (Qin et al., 1998; Yu et al., 2001).

Studies of key loess sites from the CLP confirm that accumulation on the CLP was accelerated during glacial periods compared to interglacial periods (e.g. Liu, 1985b; Kukla et al., 1988; Kukla and An, 1989; An and Xiao, 1990; An et al., 1991). However very few studies actually quantify changes in mass accumulation rates on the CLP. The quantitative estimates that do exist are derived from only a handful of sites. An et al. (1991) and Beer et al. (1993) estimate a 3-fold change on sections near Luochuan. Broecker (1995) suggests that rates changed by "nearly an order of magnitude" on the central plateau, from peak glacial to peak interglacial, and a similar order of change has been assumed by recent modeling studies (Reader et al., 1999). Our results, based on many records across the CLP, suggest that the interglacial-glacial increase was of the order of 2–4. This range encompasses the uncertainties due to the different dating techniques used to erect age models and the differences in MAR estimates for different glacials and interglacials/interstadials. The larger interglacial-glacial changes recorded at some sites (e.g. Chenjiawo/Lantian_1), and particularly at terrace sites (e.g. Zhaitang and Mangshan), are not typical of the CLP as a whole. Comparisons of such atypical sites with e.g. records from marine cores (which reflect a dust deposition signal averaged over a rather large region) are likely to yield an unrealistic picture of the gradients in palaeo-wind regimes associated with dust transportation

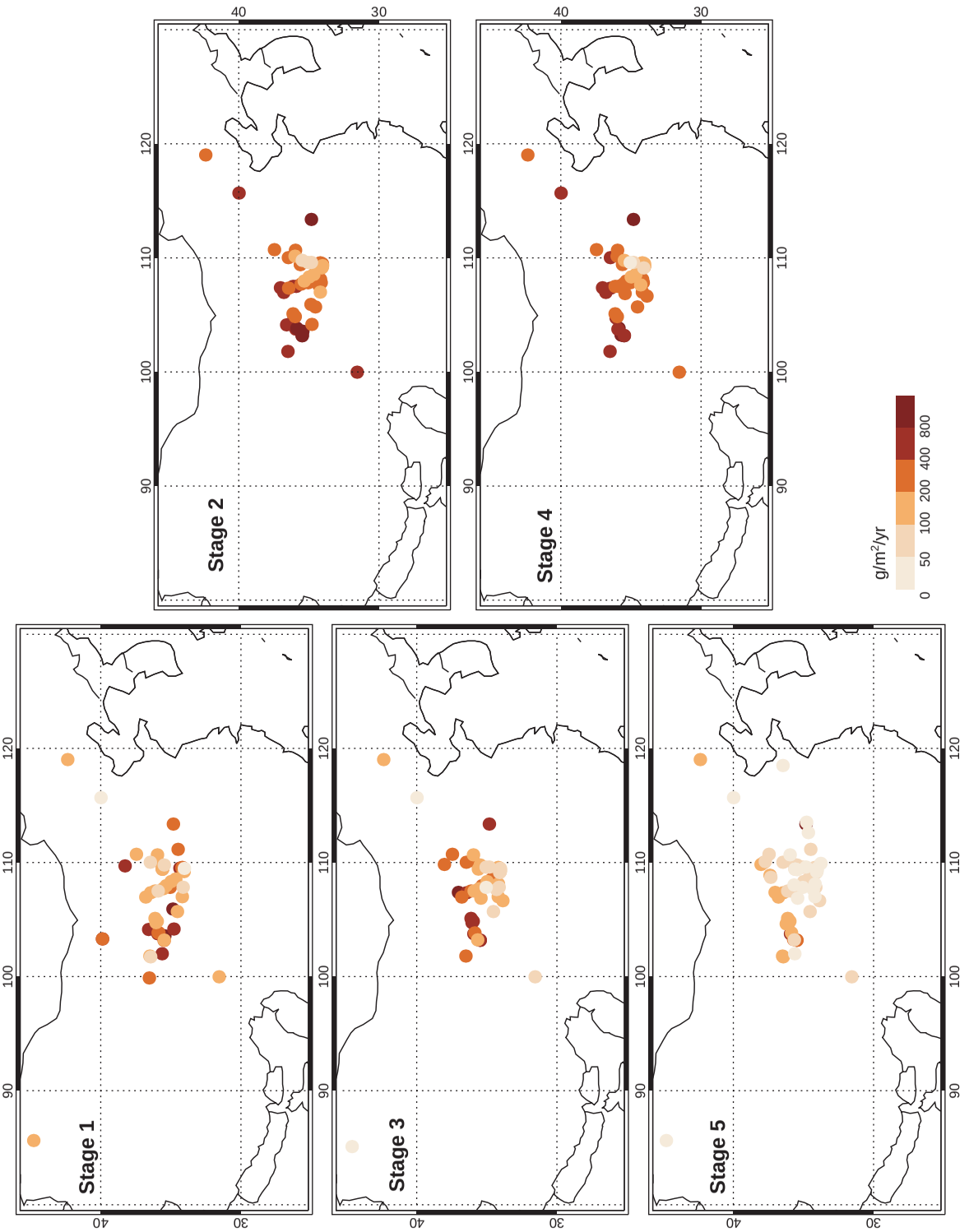

Fig. 4. MAR ($g/m^2/yr$) estimates at individual sites, based on averaging the estimates derived from different age models, for marine isotope stages 1–5.

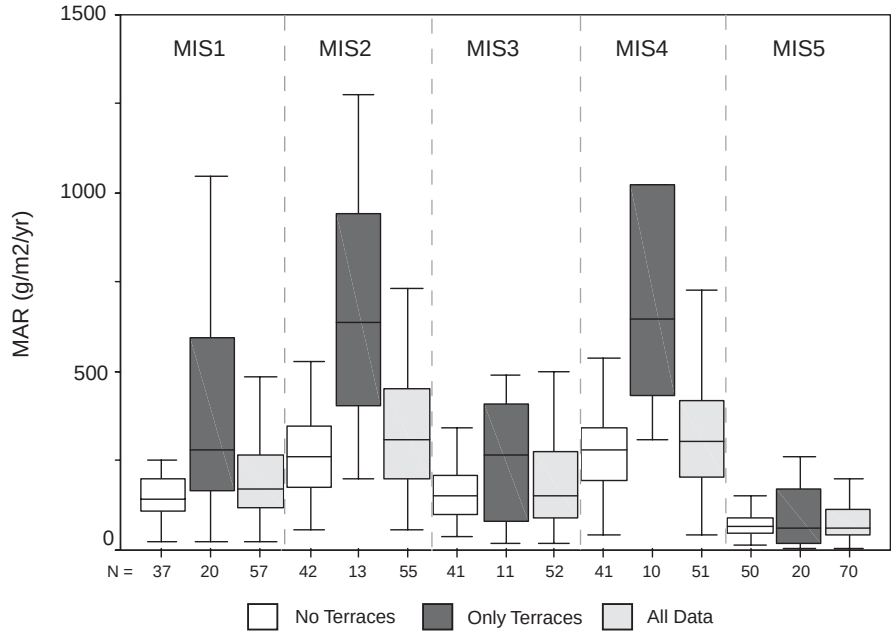

Fig. 5. Regional estimates of MAR for marine isotope stages 1–5 based on all sites compared with loess–terrace sites and all other sites respectively. Box-and-whisker presentation as in Fig. 2. Numbers at the bottom of each column indicate the number of samples.

Table 4
Regional MARs ($g/m^2/yr$) for different landforms

	Stage	Median	Mean	min	max	*N*
No terraces	1	144	200	25	1426	37
	2	262	318	60	1719	42
	3	154	202	39	809	41
	4	281	297	44	954	41
	5	68	80	16	204	50
	Stage 2/1	2	2.78	0.6	13.8	33
	Stage 2/5	3.95	4.39	0.8	16.4	40
Terraces	1	281	424	25	1298	20
	2	637	997	205	5238	13
	3	269	250	21	491	11
	4	648	935	312	2279	10
	5	62	169	6	1330	20
	Stage 2/1	3.75	6.26	0.4	24.5	10
	Stage 2/5	8	9.55	3.1	22.6	8

and loess formation. Furthermore, it should not be assumed that MARs from such sites can be generalised to yield plausible regional estimates of atmospheric dust loadings during specific periods. This is a crucial issue if the MARs from loess deposits are to be used to evaluate model simulations of the palaeo-dust cycle. The current generation of dust cycle models have a rather coarse spatial resolution (ca $4^\circ \times 5^\circ$) (Tegen, 2003) and thus can only be expected to predict the average change in dust loading over relatively large regions (Harrison et al., 2001a). Our analyses show that it is important for regional estimates to be generated from a large suite of sites, rather than by extrapolation of MARs estimated at individual sites which, because of their geomorphic setting or their geographic location, could have atypically high MARs.

4.2. Causes of differences in MARs between interglacial periods

The MAR estimates for the current interglacial (Stage 1) are considerably higher than those for the last interglacial period (Stage 5). Northern hemisphere incoming solar radiation (insolation) receipts during summer were higher during the peak of Stage 5 than during the peak of the present interglacial (Berger, 1978), which would result in stronger monsoon development (Kutzbach, 1981; Joussaume et al., 1999). A much-expanded Pacific monsoon might have reduced the extent of desert sources outside the CLP and would certainly have minimised loess recycling within the CLP. Thus, the observed difference between MARs during the last and the current interglacial could be a reflection of differences in the climate of central Asia and the CLP between the two interglacials. However, this does not provide a satisfactory explanation for the fact that Stage 1 MARs are slightly higher than those for the last interstadial (Stage 3). It therefore seems likely that our estimates for Stage 1 are inflated. There are several possible factors that could cause an inflation of the Stage 1 MAR estimates: biases in the nature of the sites sampled, biases in the dating technique, biases due to the unequal length of the sampling period, and possible human impact on accumulation.

There are potential biases in our estimates of Stage 1 MARs. Except during Stage 5, terrace sites have significantly higher accumulation rates than non-terrace sites. About 36% of the sites yielding Stage 1 MARs are loess terraces; terrace sites are much less important in the calculation of the average MAR for other stages. Only 29% of the sites yielding Stage 5 MARs are loess terraces. The MAR for Stage 1, estimated for non-terrace sites, is 144 g/m^2/yr. This is still substantially higher than the estimated Stage 5 MAR. However, this estimate indicates Stage 1 MARs comparable to the MAR for the interstadial (Stage 3). Correlation-dating techniques (pedostratigraphy, magnetic susceptibility) tend to yield lower MAR estimates for interglacial periods than absolute dating techniques. Most of the records (89%) for Stage 5 are based entirely on correlation-dating, whereas 35% of the records for Stage 1 incorporate absolute dating techniques. This would yield higher Stage 1 MARs and hence tend to inflate the overall average. Finally, the Stage 5 MARs are estimates of the average accumulation over a rather long period (56 kyr) whereas the Stage 1 estimates are averages over only 12 kyr. Aeolian accumulation rates have varied by a factor of 2 during Stage 1. The dating control is insufficient to make a similar estimate for Stage 5, although it is plausible to suggest that the last interglacial period was also characterised by similar millennial-scale variability. If this were the case, then the average MAR could be significantly influenced by the length of the sampling period considered. The impact of these biases could be minimised were it possible to calculate MARs for the different marine isotope stages based on a specific type of site, using the same dating method, and averaging over a similar period. Unfortunately, such rigid selection procedures would result in

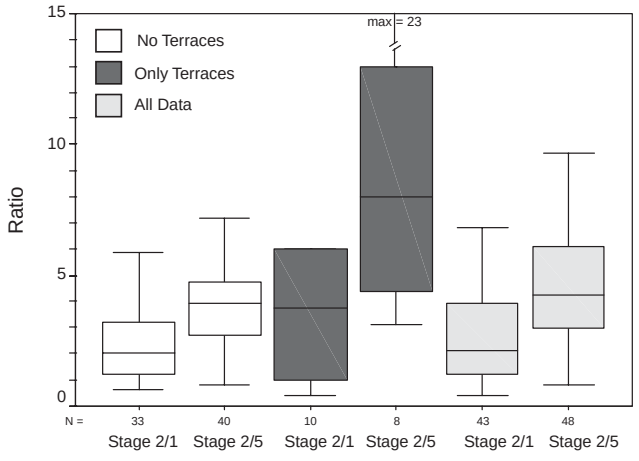

Fig. 6. Differences in deposition flux ratios for Stage 2/Stage 1 and Stage 2/5 between terrace and non-terrace sites. Box-and-whisker presentation as in Fig. 2. Numbers at the bottom of each column indicate the number of samples.

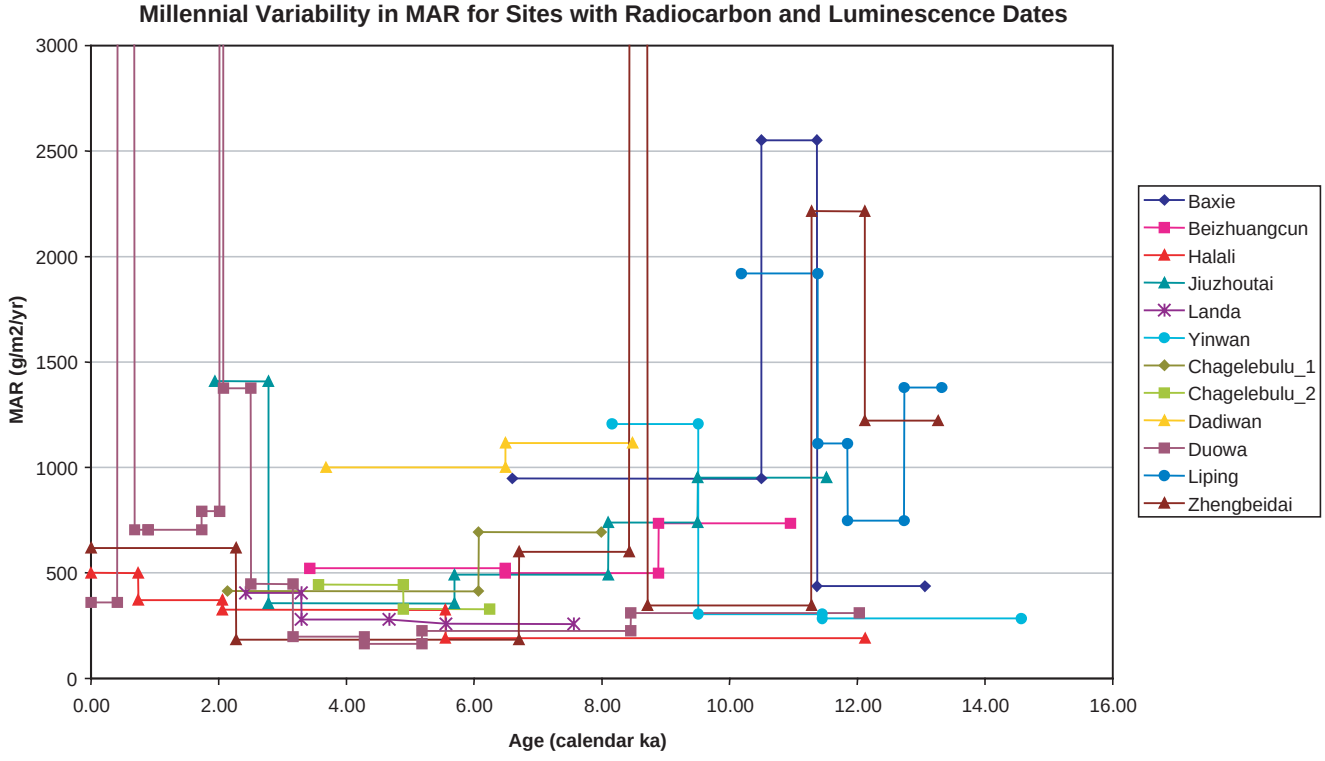

Fig. 7. Changes in MAR at individual, radiometrically dated sites during the last 14 calendar kyr. MAR estimates were made for each interval with bracketing radiocarbon dates, where the symbols indicate the radiocarbon dates available at each site.

the loss of most of the MAR estimates currently available, resulting in the production of regional average changes based on a handful of sites.

We did not calculate Stage 1 MARs when the presence of a cultivation layer indicated that the site record was directly impacted by human activities. Cultivation would tend to remove loess material and thus such sites would be likely to have lower-than-expected accumulation rates. Human-induced changes in the regional vegetation cover and agricultural practices that cause the soil to be exposed to deflation during the critical spring period, however, could increase recycling of loess-derived material within the CLP and thus increase deposition at non-cultivated sites. Archaeological and pollen evidence suggest that agricultural activity on the CLP began ca 5–6000 years ago (Ren, 2000). Furthermore, a well-dated, high-resolution record from the western CLP shows a 6-fold increase in dust accumulation rates ca 2500 yr B.P. associated with changes in agricultural practices (Roberts et al., 2001). These observations make it plausible that our Stage 1 MAR estimates are inflated because of human activities.

4.3. Source of CLP loess

There are thought to be three sources for the loess that comprises the CLP (Smalley and Krinsley, 1978; Derbyshire, 1983; Gallet et al., 1998; Wright, 2001): silt-sized material derived from adjacent deserts, glacially derived material from the surrounding mountains, and recycling of older loess which has been fluvially transported and deposited in river valleys within the CLP. The deserts lying to the north and west of the CLP are major centres of dust storm activity during the late winter and spring today (Pye and Zhou, 1989; Zhang et al., 1997; Sun et al., 2000b). These deserts include western source regions in eastern Xinjiang (e.g. Taklamakan, Kumutage and Qaidam Basin), and deserts more directly north of the CLP in eastern Gansu and western Inner Mongolia (e.g. Ulanbuh, Tengger, and Badainjuran Deserts). Much of the dust reaching the CLP today appears to be derived from these deserts and transported through the Hexi Corridor in the northwest of the CLP (Derbyshire et al., 1998). Deserts in eastern Inner Mongolia (e.g. Ordos, Hobq, and Mu Us) may also contribute small amounts of dust to the CLP.

The spatial patterns in MAR, with highest values in the northwest of the CLP and lowest values in the southeast during all isotope stages, suggest that these sources have been dominant throughout the last interglacial–glacial–interglacial cycle. Thus, the results of our analyses are consistent with previous interpretations (see e.g. Derbyshire et al., 1998) that deserts have been the dominant source of material for the CLP and that the transportation pathway for this material has been from northwest to southeast. Glacial deposits in the mountain regions surrounding the CLP may have provided an additional source of dust (see e.g. Smalley and Krinsley, 1978; Wright, 2001), particularly during interglacials when the glaciers were less extensive and thus the glacial deposits were exposed for aeolian reworking. The sources of this glacial dust also lie to the northwest of the CLP, and are therefore unlikely to modify the spatial patterns in dust accumulation determined by the desert sources to the northwest.

Both the MAR estimates for individual sites (Table 2) and the regional median values provide strong support for the importance of local recycling of material within the CLP. Terrace sites have much higher MARs than non-terrace sites (Fig. 5; Table 4), such that the regional MARs for Stages 2 and 4 terraces are 2.3–2.4 times larger than the MARs for non-terrace sites. Differences between MARs for terrace and non-terrace sites are smaller during interglacial/interstadial periods, and non-existent for Stage 5. This implies that the aeolian recycling of loessic material occurred primarily during the glacial periods. This is indeed consistent with the broad outline of climate changes on the CLP, with wetter climates (favouring fluvial transport of loess) during interglacials, and cold and dry conditions (favouring reworking of the sediments exposed in river channels) during glacial periods (Wang et al., 1999).

4.4. Millennial-scale variability in MAR

Absolutely dated high resolution records of MAR during Stage 1 show that there are significant millennial-scale variations in dust accumulation. The records show high dust accumulation during the late glacial and early Holocene and lowest accumulation rates between ca 7000 and 3000 yr B.P. The dust minimum roughly corresponds with other records that show a maximum expansion of the Pacific monsoon during the mid-Holocene, with millennial-scale oscillations superimposed on the general trend (e.g. Shi et al., 1993; An et al., 2000; Guo et al., 2000; Zhang et al., 2000). The timing of the onset of reduced dust accumulation varies from site to site, and may reflect spatial patterning in the timing of increased monsoonal rainfall (see e.g. An et al., 2000). Additional high-resolution records are required to address this issue. Nevertheless, the existing records suggest that there is a considerable lag between the changes in orbital forcing that ultimately drive changes in the monsoon (Winkler and Wang, 1993) and the response of regional climates as reflected in changes in the dust cycle. Investigations of the mechanisms underlying this lagged response could provide insights into the feedbacks involved in regional climate change.

The assumptions underlying the use of pedostratigraphy as a dating technique effectively precludes any

examination of potential lags between climate forcings and regional responses during earlier phases of the dust record. It has been suggested (e.g. Heller and Evans, 1995; Chen et al., 1997; Heslop et al., 1999) that variations in magnetic susceptibility are indicative of millennial-scale changes in climate variability. The poor correlations between individual magnetic susceptibility records from the CLP and the marine isotope stratigraphy during the last 150 kyr, however, suggest that the utility of magnetic susceptibility as a dating technique is limited (see e.g. Heslop et al., 2000). Independent dating control is needed to investigate how millennial changes in magnetic susceptibility relate to the global climate. Further investigations of the millennial-scale variability in the dust cycle prior to Stage 1 will require a substantial improvement to both the quality and the quantity of absolutely-dated records from the CLP.

5. Conclusions

Estimates of MAR from the CLP show qualitatively robust temporal and spatial patterns. Glacial periods are characterised by higher dust accumulation than interglacial periods. The highest rates of dust accumulation occur in the northwest of the CLP, close to potential desert sources, and are lowest in the southeast. Loess terraces consistently yield higher estimates of dust deposition than other sites, indicating that dust recycling from local sources within the CLP has been important throughout the last interglacial–glacial–interglacial cycle.

There are large uncertainties attached to the magnitude of glacial–interglacial changes in dust accumulation. The lack of bulk density measurements on individual loess sections, for example, necessitates the use of a generic value for bulk density, which could change the MAR estimates by $\pm 15\%$. The estimated MAR for a given stage at an individual site is affected by the choice of dating technique used to erect an age model. The estimation uncertainty due to the choice of age model can be as large as 192%. Regional estimates of MAR during individual stages are affected by biases in sampling, both as a result of the differential availability of absolute versus correlation-based chronologies and as a result of differences in the type of sites from which records are available through time. Insufficient records are currently available from the CLP to exclude such sampling biases in a rigorous way. Finally, it seems likely that changes in dust deposition during the later part of the Holocene have been affected by anthropogenically-induced landscape changes. The magnitude of this impact on estimates of Stage 1 MARs is uncertain. Thus, although the CLP represents perhaps the best-studied loess region in the world, there is still much to do to quantify changes in MAR during the last interglacial–glacial–interglacial cycle.

Nevertheless, the data synthesised here present a number of concrete challenges to the dust modelling community. Specifically:

- The regional increase in dust deposition from glacial to interglacial across the CLP is between 2.1 and 4.3. Existing, coarse-resolution models of the dust cycle should be able to reproduce this change.
- Spatial gradients in MAR show that dust sources lying northwest of the CLP have been important throughout the last interglacial–glacial–interglacial cycle. Existing models of the dust cycle should be able to reproduce the location of these sources.
- Dust recycling within the CLP affects MAR estimates at individual sites and, in particular, results in higher dust accumulation close to rivers. Existing models of the dust cycle cannot be expected to resolve such small-scale patterns. However, the latest generation of source-area models (e.g. Tegen, 2003; Tegen et al., 2002) predict local dust sources from geomorphically-favourable sites such as former lake basins. This approach could equally well be applied to local sources of dust within river channels. Although, the simulation of dust accumulation at individual terrace sites would require a considerable increase in the spatial resolution used for source-area modelling, it should be possible to predict the regional difference in deposition between sites that are influenced by local river sources and sites that are not affected by such sources (i.e. the regional difference between terrace and non-terrace sites). According to our analyses, terraces should show a 3.8 to 8-fold increase in deposition whereas non-terrace sites should show only a 2 to 4-fold increase between glacial and interglacial periods.

Acknowledgements

We thank W.J. Zhou for kindly and quickly providing data and information. We also thank S. Stanek, G. Boenisch for their assistance with graphics and database management. We thank D. Heslop and R. Kemp for their helpful reviews. This work was completed as part of the DIRTMAP Data Base, which is funded through the MPI-BGC. The MPI-BGC also provided financial support for J.M. Sun who assisted with data compilation from March to October, 1999. The DIRTMAP database (http://www.bgc-jena.mpg.de/bgc_prentice) is endorsed and supported by the INQUA Loess Commission, the IGBP/GAIM Paleo Trace Gas and Mineral Aerosol Challenge (TRACES), the IGBP/PAGES PaleoMApping Project (PMAP), and the International Geological Correlation Programme (IGCP) #413. The members of the DIRTMAP Steering Committee are E. Derbyshire, S.P. Harrison, P. Hesse, D. Muhs, A. Wintle, and L. Zhou.

References

Aitken, M.J., 1998. An Introduction to Optical Dating: The Dating of Quaternary Sediments by the Use of Photon-stimulated Luminescence. Oxford University Press, Oxford, UK.

An, Z.S., 2000. The history and variability of East Asian Paleomonsoon climate. Quaternary Science Reviews 19, 171–187.

An, Z., Porter, S.C., 1997. Millennial-scale climatic oscillations during the last interglaciation in central China. Geology 25, 603–606.

An, Z.S., Sun, D.H., 1995. Discussion of the monsoon variation over the Loess Plateau in the last interglacial cycle. In: Ye, D.Z. (Ed.), China Contribution to Global Change. Science Press, Beijing, pp. 122–124.

An, Z.S., Xiao, J.L., 1990. A real example about the study of dust sedimentary flux in the loess plateau. Geoderma 45, 123–143.

An, Z.S., Kukla, G., Porter, S.C., Xiao, J.L., 1991. Late Quaternary dust flow on the Chinese Loess Plateau. Catena 18, 125–132.

An, Z.S., Wang, S.M., Wu, X.H., Cheng, M.Y., Sun, D.H., Liu, X.M., Wang, F.B., Li, L., Sun, Y.B., Zhou, W.J., Zhou, J., Liu, X.D., Lu, H.Y., Zhang, Y.X., Dong, G.R., Qiang, X.K., 1999. Eolian evidence from the Chinese Loess Plateau: the onset of the Late Cenozoic Great Glaciation in the North Hemisphere and Qinghai-Xizang Plateau uplift forcing. Science in China, Series D 42, 258–271.

An, Z.S., Porter, S.C., Kutzbach, J.E., Wu, X.H., Wang, S.M., Liu, X.D., Li, X.Q., Zhou, W.J., 2000. Asynchronous Holocene optimum of the East Asian monsoon. Quaternary Science Reviews 19, 743–762.

Beer, J., Shen, C., Heller, F., Liu, T., Bonani, G., Dittrich, B., Suter, M., Kubik, P.W., 1993. ^{10}Be and magnetic susceptibility in Chinese loess. Geophysical Research Letters 20, 57–60.

Berger, A.L., 1978. Long-term variations of caloric insolation resulting from the Earth's orbital elements. Quaternary Research 9, 139–167.

Berger, G.W., 1988. Tl dating studies of tephra, loess and lacustrine sediments. Quaternary Science Reviews 7, 295–303.

Berger, G.W., Pillans, B.J., Palmer, A.S., 1992. Dating loess up to 800 ka by thermoluminescence. Geology 20, 403–406.

Broecker, W.S., 1995. The Glacial World According to Wally. Eldigio Press, Lamont-Doherty Earth Observatory of Columbia University, Palisades, NY.

Chen, F.H., Bloemendal, J., Wang, J.M., Li, J.J., Oldfield, F., 1997. High-resolution multi-proxy climate records from Chinese loess: evidence for rapid climatic changes over the last 75 kyr. Palaeogeography, Palaeoclimatology, Palaeoecology 130, 323–335.

Chen, J., An, Z., Head, J., 1999. Variation of RB/Sr ratios in the loess-paleosol sequences of Central China during the last 130,000 years and their implications for monsoon paleoclimatology. Quaternary Research 51, 215–219.

Clemens, S.C., Prell, W.L., 1990. Late Pleistocene variability of Arabian Sea summer monsoon winds and continental aridity: eolian records from the lithogenic component of deep-sea sediments. Paleoceanography 5, 109–145.

Cragin, J.H., Herron Jr., M.M., Klouda, C.C.L., 1977. Interhemispheric comparison of changes in the composition of atmospheric precipitation during the late Cenozoic era. In: Dunbar, M.J. (Ed.), Polar Oceans, Proceedings of the Polar Oceans Conference. Arctic Institute of North America, Calgary, Ala, pp. 617–641.

De Angelis, M., Legrand, M., Petit, J.R., Barkov, N.I., Korotkevitch, Y.S., Kotlyakov, V.M., 1984. Soluble and insoluble impurities along the 950 m deep Vostok ice core (Antarctica)—climate implications. Journal of Atmospheric Chemistry 1, 215–239.

Derbyshire, E., 1983. On the morphology, sediments, and origin of the Loess Plateau of central China. In: Gardner, R., Scoging, H. (Eds.), Mega-geomorphology; Conference of the British Geomorphological Research Group. Oxford University Press, Oxford, pp. 172–194.

Derbyshire, E., Kemp, R., Meng, X., 1995. Variations in loess and palaeosol properties as indicators of palaeoclimatic gradients across the Loess Plateau of North China. Quaternary Science Reviews 14, 681–697.

Derbyshire, E., Meng, X., Kemp, R.A., 1998. Provenance, transport and characteristics of modern aeolian dust in western Gansu Province, China, and interpretation of the Quaternary loess record. Journal of Arid Environments 39, 497–516.

Derbyshire, E., Meng, X.M., Dijkstra, T.A., 2000. Landslides in the Thick Loess Terrain of North-West China. Wiley, Chichester, pp. 81–87.

Ding, Z.L., Rutter, N., Liu, T.S., Evans, M.E., Wang, Y.C., 1991. Climatic correlation between Chinese loess and deep-sea cores: a structural approach. In: Liu, T.S. (Ed.), Loess, Environment and Global Change. Science Press, Beijing, pp. 168–186.

Ding, Z.L., Sun, J.M., Liu, T.S., Zhu, R.X., Yang, S.L., Guo, B., 1998. Wind-blown origin of the Pliocene red clay formation in the central Loess Plateau, China. Earth and Planetary Science Letters 161, 135–143.

Ding, Z.L., Xiong, S.F., Sun, J.M., Yang, S.L., Gu, Z.Y., Liu, T.S., 1999. Pedostratigraphy and paleomagnetism of a similar to 7.0 Ma eolian loess-red clay sequence at Lingtai, Loess Plateau, north-central China and the implications for paleomonsoon evolution. Palaeogeography, Palaeoclimatology, Palaeoecology 152, 49–66.

Ding, Z.L., Yang, S.L., Sun, J.M., Liu, T.S., 2001. Iron geochemistry of loess and red clay deposits in the Chinese Loess Plateau and implications for long-term Asian monsoon evolution in the last 7.0 Ma. Earth and Planetary Science Letters 185, 99–109.

Elenga, H., Peryon, O., Bonnefille, R., Prentice, I.C., Jolly, D., Cheddadi, R., Guiot, J., Andrieu, V., Bottema, S., Buchet, G.-L., de Beaulieu, J.L., Hamilton, A.C., Maley, J., Marchant, R., Perez-Obiol, R., Reille, M., Riollet, G., Scott, L., Straka, H., Taylor, D., Van Campo, E., Vincens, A., Laarif, F., Jonson, H., 2000. Pollen-based reconstruction for Southern Europe and Africa 18,000 years ago. Journal of Biogeography 27, 621–634.

Fang, X.M., Dai, X.R., Li, J.J., Cao, J.X., Guan, D.H., He, Y.P., Wang, J.L., Wang, J.P., 1996. The mutability and instability of the East Asian monsoon evolution—evidence derived from the last interglacial soil (in Chinese). Science in China Series D 26, 154–160.

Fisher, D.A., 1979. Comparison of 105 years of oxygen isotope and insoluble impurity profiles from the Devon Island and Camp Century ice cores. Quaternary Research 11, 299–305.

Frechen, M., Dodonov, A.E., 1998. Loess chronology of the last interglacial/glacial cycle in Central Asia. Geologische Rundschau 87, 2–20.

Gallet, S., Jahn, B., Van Vliet Lanoë, B., Dia, A., Rosselo, E., 1998. Loess geochemistry and its implications for particle origin and composition of the upper continental crust. Earth and Planetary Science Letters 156, 157–172.

Gu, Z.Y., Lal, D., Liu, T.S., Guo, Z.T., Southon, J., Caffee, M.W., 1997. Weathering histories of Chinese loess deposits based on Uranium and Thorium series nuclides and cosmogenic ^{10}Be. Geochimica et Cosmochemica Acta 61, 5221–5231.

Guo, Z., Fedoroff, N., An, Z.S., Liu, T.S., 1993. Interglacial dustfall and origin of iron oxides-hydroxides in the paleosols of the Xifeng loess section, China. Scientia Geologica Sinica 2, 91–100.

Guo, Z.T., Petit-Maire, N., Kröpelin, S., 2000. Holocene non-orbital climatic events in present-day arid areas of northern Africa and China. Global and Planetary Change 26, 97–103.

Hammer, C.U., 1977. Dust studies on Greenland ice cores. In: Isotopes and impurities in snow and ice—Symposium. Proceedings of the Grenoble Symposium, pp. 365–370.

Hammer, C.U., Clausen, H.B., Dansgaard, W., Neftel, A., Kristinsdottor, P., Johnson, E., 1985. Continuous impurity analysis along the Dye 3 deep core. In: Langway Jr., C., Oeschger, H., Dansgaard, W. (Eds.), Greenland Ice Core: Geophysics, Geochemistry, and

the Environment. Geophys. Monogr. AGU, Washington DC, pp. 90–94.
Harrison, S.P., Kohfeld, K.E., Roelandt, C., Claquin, T., 2001a. The role of dust in climate changes today, at the last glacial maximum and in the future. Earth Science Reviews 54, 43–80.
Harrison, S.P., Yu, G., Takahara, H., Prentice, I.C., 2001b. Palaeovegetation—diversity of temperate plants in east Asia. Nature 413, 129–130.
Heller, F., Evans, M.E., 1995. Loess magnetism. Reviews of Geophysics 33, 211–240.
Heslop, D., Shaw, J., Bloemendal, J., Chen, F., Wang, J., Parker, E., 1999. Sub-millennial scale variations in East Asian monsoon systems recorded by dust deposits from the north-western Chinese Loess Plateau. Physics of the Earth and Planetary Interiors 24, 785–792.
Heslop, D., Langereis, C.G., Dekkers, M.J., 2000. A new astronomical timescale for the loess deposits of Northern China. Earth and Planetary Science Letters 184, 125–139.
Hovan, S.A., Rea, D.K., Pisias, N.G., 1991. Late Pleistocene continental climate and oceanic variability recorded in Northwest Pacific sediments. Paleoceanography 6, 349–370.
Joussaume, S., Taylor, K.E., Braconnot, P., Mitchell, J.F.B., Kutzbach, J., Harrison, S.P., Prentice, I.C., Broccoli, A.J., Abe-Ouchi, A., Bartlein, P.J., Bonfils, C., Dong, B., Guiot, J., Herterich, K., Hewitt, C.D., Jolly, D., Kim, J.W., Kislov, A., Kitoh, A., Loutre, M.F., Masson, V., McAvaney, B., McFarlane, N., deNoblet, N., Peltier, W.R., Peterschmitt, J.Y., Pollard, D., Rind, D., Royer, J.F., Schlesinger, M.E., Syktus, J., Thompson, S., Valdes, P., Vettoretti, G., Webb, R.S., Wyputta, U., 1999. Monsoon changes for 6000 years ago: results of 18 simulations from the Paleoclimate Modeling Intercomparison Project (PMIP). Geophysical Research Letters 26, 859–862.
Kohfeld, K.E., Harrison, S.P., 2001. Dirtmap: the geologic record of dust. Earth Science Reviews 54, 81–114.
Kukla, G., An, Z., 1989. Loess stratigraphy in central China. Palaeogeography, Palaeoclimatology, Palaeoecology 72, 203–225.
Kukla, G., Heller, F., Ming, L.X., Chun, X.T., Sheng, L.T., Sheng, A.Z., 1988. Pleistocene climates in China dated by magnetic susceptibility. Geology 16, 811–814.
Kutzbach, J.E., 1981. Monsoon climate of the early Holocene: climate experiment with the earth's orbital parameters for 9000 years ago. Science 214, 59–61.
Lai, Z.P., Singhvi, A., Chen, H.Z., Zhou, W.J., 1999. Luminescence chronology of Holocene sediments from Taipingchuan in the Loess/Desert transitional zone, China and its implications. Man and Environment 14, 91–97.
Liu, T.S., 1964. Loess on the Middle Reaches of the Yellow River. Science Press, Beijing, China (in Chinese).
Liu, T.S., 1965. The Loess Deposits in China. Science Press, Beijing (in Chinese).
Liu, T.S., 1966. Composition and Texture of Loess. Science Press, Beijing (in Chinese).
Liu, T., 1985a. Loess in China. China Ocean Press Beijing/Springer, Beijing/Berlin.
Liu, T.S., 1985b. Loess and the Environment. China Ocean Press, Beijing (in Chinese).
Liu, T., An, Z., Yuan, B., Han, J., 1985. The loess–paleosol sequence in China and climatic history. Episodes 8, 21–28.
Liu, T.S., An, Z.S., Cheng, M.Y., Sun, D.H., 1996. A correlation between southern and northern hemispheres during the last 0.6 MA. Science in China, Series D 39, 113–120.
Lu, H.Y., van Huissteden, K., An, Z.S., Nugteren, G., Vandenberghe, J., 1999. East Asia winter monsoon variations on a millenial timescale before the last glacial–interglacial cycle. Journal of Quaternary Science 14, 101–110.
Mahowald, N., Kohfeld, K.E., Hansson, M., Balkanski, Y., Harrison, S.P., Prentice, I.C., Schulz, M., Rodhe, H., 1999. Dust sources and deposition during the Last Glacial maximum and current climate: a comparison of model results with palaeodata from ice cores and marine sediments. Journal of Geophysical Research 104, 15895–15916.
Martinson, D.G., Pisias, N.G., Hays, J.D., Imbrie, J., Moore, T.C., Shackleton, N.J., 1987. Age dating and the orbital theory of the ice ages—development of a high-resolution 0 to 300,000-year chronostratigraphy. Quaternary Research 27, 1–29.
Muhs, D.R., Aleinikoff, J.N., Stafford Jr., T.W., Kihl, R., Been, J., Mahan, S.A., 1999. Late Quaternary loess in northeastern Colorado. I. Age and paleoclimatic significance. Geological Society of America Bulletin 111, 1861–1875.
Paillard, D., Labeyrie, L., Yiou, P., 1996. Macintosh program performs time-series analysis. Eos Transactions AGU 77, 379.
Petit, J.R., Briat, M., Royer, A., 1981. Ice age aerosol content from East Antarctic ice core samples and past wind strength. Nature 293, 391–394.
Petit, J.R., Mounier, L., Jouzel, J., Korotkevich, Y.S., Kotlyakov, V.I., Lorius, C., 1990. Paleoclimatological and chronological implications of the Vostok core dust record. Nature 343, 56–58.
Petit, J.R., Jouzel, J., Raynaud, D., Barkov, N.I., Barnola, J.M., Basile, I., Bender, M., Chappellaz, J., Davis, M., Delaygue, G., Delmotte, M., Kotlyakov, V.M., Legrand, M., Lipenkov, V.Y., Lorius, C., Pepin, L., Ritz, C., Saltzman, E., Stievenard, M., 1999. Climate and atmospheric history of the past 420,000 years from the Vostok ice core, Antarctica. Nature 399, 436–439.
Pye, K., 1987. Aeolian Dust and Dust Deposits. Academic Press, San Diego.
Pye, K., Zhou, L.-P., 1989. Late Pleistocene and Holocene aeolian dust deposition in North China and the northwest Pacific Ocean. Palaeogeography, Palaeoclimatology, Palaeoecology 73, 11–23.
Qin, B., Harrison, S.P., Kutzbach, J.E., 1998. Evaluation of modelled regional water balance using lake status data: a comparison of 6 ka simulations with the NCAR CCM. Quaternary Science Reviews 17, 535–548.
Rea, D.K., 1990. Aspects of atmospheric circulation: the Late Pleistocene (0–950,000 yr) record of eolian deposition in the Pacific Ocean. Palaeogeography, Palaeoclimatology, Palaeoecology 78, 217–227.
Rea, D.K., 1994. The paleoclimatic record provided by eolian deposition in the deep sea: the geologic history of wind. Reviews of Geophysics 32, 159–195.
Reader, M.C., Fung, I., McFarlane, N., 1999. The mineral dust aerosol cycle during the Last Glacial Maximum. Journal of Geophysical Research—Atmospheres 104, 9381–9398.
Reader, M.C., Fung, I., McFarlane, N., 2000. Mineral aerosols: a comparison of the last glacial maximum and preindustrial Holocene. Canadian Journal of Earth Sciences 37, 751–767.
Ren, G., 2000. Decline of the mid- to late Holocene forests in China: climatic change or human impact? Journal of Quaternary Science 15, 273–281.
Roberts, H.M., Wintle, A.G., Maher, B.A., Hu, M.Y., 2001. Holocene sediment-accumulation rates in the western Loess Plateau, China, and a 2500-year record of agricultural activity, revealed by OSL dating. The Holocene 11, 477–483.
Ruddiman, W.F., 1997. Tropical atlantic terrigenous fluxes since 25,000 yrs B.P. Marine Geology 136, 189–207.
Sarnthein, M., Koopman, B., 1980. Late Quaternary deep-sea record on northwest African dust supply and wind circulation. Palaeoecology of Africa 12, 239–253.
Sarnthein, M., Tetzlaff, G., Koopmann, B., Wolter, K., Pflaumann, U., 1981. Glacial and interglacial wind regimes over the eastern subtropical Atlantic and North-West Africa. Nature 293, 193–196.

Shi, Y.F., Kong, Z.Z., Wang, S.M., Tang, L.Y., Wang, F.B., Yao, T.D., Zhao, X.T., Zhang, P.Y., Shi, S.H., 1993. Mid-Holocene climates and environments in China. Global and Planetary Change 7, 219–233.

Sirocko, F., Lange, H., 1991. Clay-mineral accumulation rates in the Arabian Sea during the late Quaternary. Marine Geology 97, 105–119.

Smalley, I.J., Krinsley, D.H., 1978. Loess deposits associated with deserts. Catena 5, 53–66.

Steffensen, J.P., 1997. The size distribution of microparticles from selected segments of the Greenland Ice Core Project ice core representing different climatic periods. Journal of Geophysical Research 102, 26755–26763.

Stuiver, M., Reimer, P.J., 1993. Extended ^{14}C data base and revised Calib 3.0 ^{14}C age calibration program. Radiocarbon 35, 215–230.

Stuiver, M., Reimer, P.J., Bard, E., Beck, J.W., Burr, G.S., Hughen, K.A., Kromer, B., McCormac, G., van der Plicht, J., Spurk, M., 1998a. INTCAL98 radiocarbon age calibration, 24000–0 cal BP. Radiocarbon 40, 1041–1083.

Stuiver, M., Reimer, P.J., Braziunas, T.F., 1998b. High-precision radiocarbon age calibration for terrestrial and marine samples. Radiocarbon 40, 1127–1151.

Sun, D.H., Liu, T.S., Cheng, M.Y., An, Z.S., Shaw, J., 1997. Magnetostratigraphy and paleoclimate of Red Clay sequences from the Chinese Loess Plateau. Science in China, Series D 40, 337–343.

Sun, D.H., An, Z.S., Shaw, J., Bloemendal, J., Sun, Y.B., 1998a. Magnetostratigraphy and palaeoclimatic significance of Late Tertiary aeolian sequences in the Chinese Loess Plateau. Geophysical Journal International 134, 207–212.

Sun, D.H., Shaw, J., An, Z.S., Cheng, M.Y., Yue, L.P., 1998b. Magnetostratigraphy and paleoclimatic interpretation of a continuous 7.2 Ma Late Cenozoic eolian sediments from the Chinese Loess Plateau. Geophysical Research Letters 25, 85–88.

Sun, J., Yin, G., Ding, Z., Liu, T., Chen, J., 1998c. Thermoluminescence chronology of sand profiles in the Mu Us Desert, China. Palaeogeography, Palaeoclimatology, Palaeoecology 144, 225–233.

Sun, J.M., Ding, Z.L., Liu, T.S., Rokosh, D., Rutter, N., 1999. 580,000 Year environmental reconstruction for eolian deposits at the Mu Us desert margin China. Quaternary Science Reviews 18, 1351–1364.

Sun, J., Kohfeld, K.E., Harrison, S.P., 2000a. Records of aeolian dust deposition on the Chinese Loess Plateau during the Late Quaternary. Technical Reports—Max-Planck-Institut für Biogeochemie 1, 318.

Sun, J.M., Liu, T.S., Lei, Z.F., 2000b. Sources of heavy dust fall in Beijing, China, on April 16, 1998. Geophysical Research Letters 27, 2105–2108.

Tarasov, P.E., Volkova, V.S., Webb, T., Guiot, J., Andreev, A.A., Bezusko, L.G., Bezusko, T.V., Bykova, G.V., Dorofeyuk, N.I., Kvavadze, E.V., Osipova, I.M., Panova, N.K., Sevastyanov, D.V., 2000. Last glacial maximum biomes reconstructed from pollen and plant macrofossil data from northern Eurasia. Journal of Biogeography 27, 609–620.

Tegen, I., 2003. Modeling the mineral dust aerosol cycle in the climate system. Quaternary Science Reviews, this issue (doi:10.1016/S0277-3791(03)00163-X).

Tegen, I., Harrison, S., Kohfeld, K., Prentice, I., Coe, M., Heimann, M., 2002. Impact of vegetation and preferential source areas on the dust aerosol cycle. Journal of Geophysical Research 107, 4576, doi:10.1029/2001JD000963.

Thiede, J., 1979. Wind regimes over the late Quaternary southwest Pacific Ocean. Geology 7, 259–262.

Thompson, L.G., 1977. Variations in microparticle concentration, size distribution and elemental composition fround in Camp Century, Greenland and Byrd Station, Antarctica, deep ice cores. In: Proceedings of the Grenoble Symposium on Isotopes and Impurities in Snow and Ice, IAHS-AISH, pp. 351–364.

Wang, L.J., Sarnthein, M., Grootes, P.M., Erlenkeuser, H., 1999. Millennial reoccurrence of century-scale abrupt events of East Asian monsoon: a possible heat conveyor for the global deglaciation. Paleoceanography 14, 725–731.

Winkler, M.G., Wang, P.K., 1993. The Late-Quaternary vegetation and climate of China. In: Wright Jr., H.E., Kutzbach, J.E., Webb III, T., Ruddiman, W.F., Street-Perrott, F.A., Bartlein, P.J. (Eds.), Global Climates Since the Last Glacial Maximum. University of Minnesota Press, Minneapolis, pp. 221–264.

Wintle, A.G., 1993a. Luminescence dating of aeolian sands: an overview. In: Pye, K., (Ed.), The Dynamics and Environmental Context of Aeolian Sedimentary Systems. Geological Society Special Publication No 72, pp. 49–58.

Wintle, A.G., 1993b. Recent developments in optical dating of sediments. Radiation Protection Dosimetry 47, 627–635.

Wintle, A.G., 1997. Luminescence dating: laboratory procedures and protocols. Radiation Measurements 27, 769–817.

Wintle, A.G., Questiaux, D.G., Roberts, R.G., Spooner, N.A., 1993. Dating loess up to 800 ka by thermoluminescence: comment and reply. Geology 21, 568–569.

Wright, J.S., 2001. Desert loess versus glacial loess quartz silt formation, source areas and sediment pathways in the formation of loess deposits. Geomorphology 36, 231–256.

Yu, G., Chen, X.D., Ni, J., Cheddadi, R., Guiot, J., Han, H.Y., Harrison, S.P., Huang, C.X., Ke, M.H., Kong, Z.C., Li, S.F., Li, W.-Y., Liew, P.-M., Liu, G.X., Liu, J.L., Liu, K.-B., Prentice, I.C., Ren, G.Y., Song, C.Q., Sugita, S., Sun, X.J., Tang, L.Y., Van Campo, E., Xia, Y.M., Xu, Q.H., Yan, S., Yang, X.D., Zhuo, Z., 2000. Palaeovegetation of China: a pollen-data-based synthesis for the mid-Holocene and the last glacial maximum. Journal of Biogeography 27, 635–664.

Yu, G., Harrison, S.P., Xue, B., 2001. Lake status records from China: Data Base Documentation. Technical Reports—Max-Planck-Institute für Biogeochemie, Vol. 4, 243pp.

Zhang, H.C., Ma, Y.Z., Wünnemann, B., Pachur, H.-J., 2000. A holocene climatic record from arid northwestern China. Palaeogeography, Palaeoclimatology, Palaeoecology 162, 389–401.

Zhang, X.Y., Arimoto, R., An, Z.S., 1997. Dust emission from Chinese desert sources linked to variations in atmospheric circulation. Journal of Geophysical Research 102, 28041–28047.

Zheng, H.B., An, Z.S., Shaw, J., 1992. New contributions to Chinese Plio-Pleistocene magnetostratigraphy. Physics of the Earth and Planetary Interiors 70, 146–153.

Zhou, W., Donahue, D.J., Porter, S.C., Jull, T.A., Xiaoqiang, L., Stuiver, M., Zhisheng, A., Matsumoto, E., Guangrong, D., 1996. Variability of monsoon climate in East Asia at the end of the Last Glaciation. Quaternary Research 46, 219–229.

Zhou, W.J., Donahue, D., Jull, A.J., 1997. Radiocarbon AMS dating of pollen concentrated from eolian sediments: implications for monsoon climate change since the late Quaternary. Radiocarbon 39, 19–26.

Zhou, W.J., An, Z.S., Jull, A.J.T., Donahue, D.J., Head, M.J., 1998. Reappraisal of Chinese Loess Plateau stratigraphic sequences over the 30,000 last years: precursors of an important Holocene monsoon climatic event. Radiocarbon 40, 905–913.

Zhou, W., Head, M.J., Lu, X., An, Z., Jull, A.J.T., Donahue, D., 1999a. Teleconnection of climatic events between East Asia and polar, high latitude areas during the last deglaciation. Palaeogeography, Palaeoclimatology, Palaeoecology 152, 163–172.

Zhou, W.J., Head, M.J., Wang, F.B., Donahue, D.J., Jull, A.J.T., 1999b. The reliability of AMS radiocarbon dating of shells from China. Radiocarbon 41, 17–24.